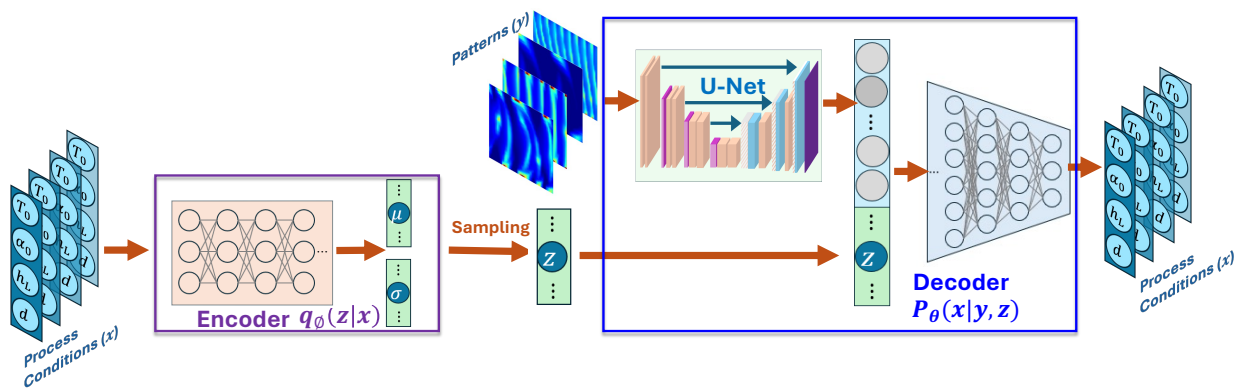


Graphical Abstract

Univariate Conditional Variational Autoencoder for Morphogenic Pattern Design in Frontal Polymerization-Based Manufacturing

Qibang Liu, Pengfei Cai, Diab Abueidda, Sagar Vyas, Seid Koric, Rafael Gomez-Bombarelli, Philippe Geubelle



Highlights

Univariate Conditional Variational Autoencoder for Morphogenic Pattern Design in Frontal Polymerization-Based Manufacturing

Qibang Liu, Pengfei Cai, Diab Abueidda, Sagar Vyas, Seid Koric, Rafael Gomez-Bombarelli, Philippe Geubelle

- A novel variational autoencoder (UcVAE) was proposed
- The UcVAE was applied to patterns design in FP-Based morphogenic manufacturing
- UcVAE saves 50% training time comparing to cVAE for patterns design

Univariate Conditional Variational Autoencoder for Morphogenic Pattern Design in Frontal Polymerization-Based Manufacturing

Qibang Liu^{a,b,c,f}, Pengfei Cai^g, Diab Abueidda^{a,e}, Sagar Vyas^{b,c}, Seid Koric^{a,d}, Rafael Gomez-Bombarelli^g and Philippe Geubelle^{b,c,*}

^aNational Center for Supercomputing Applications, University of Illinois Urbana–Champaign, Urbana, 61801, IL, USA

^bBeckman Institute for Advanced Science and Technology, University of Illinois Urbana–Champaign, Urbana, 61801, IL, USA

^cDepartment of Aerospace Engineering, Grainger College of Engineering, University of Illinois Urbana–Champaign, Urbana, 61801, IL, USA

^dDepartment of Mechanical Science and Engineering, Grainger College of Engineering, University of Illinois Urbana–Champaign, Urbana, 61801, IL, USA

^eCivil and Urban Engineering Department, New York University Abu Dhabi, United Arab Emirates

^fDepartment of Industrial and Manufacturing Systems Engineering, Kansas State University, Manhattan, 66506, KS, USA

^gDepartment of Materials Science and Engineering, Massachusetts Institute of Technology, Cambridge, 02139, MA, USA

ARTICLE INFO

Keywords:

Frontal Polymerization
Manufacturing
Inverse Design
Variational Autoencoder
Deep Learning
Deep Generative Model

ABSTRACT

Under some initial and boundary conditions, the rapid reaction-thermal diffusion process taking place during frontal polymerization (FP) destabilizes the planar mode of front propagation, leading to spatially varying, complex hierarchical patterns in thermoset polymeric materials. Although modern reaction-diffusion models can predict the patterns resulting from unstable FP, the inverse design of patterns, which aims to retrieve process conditions that produce a desired pattern, remains an open challenge due to the non-unique and non-intuitive mapping between process conditions and manufactured patterns. In this work, we propose a probabilistic generative model named univariate conditional variational autoencoder (UcVAE) for the inverse design of hierarchical patterns in FP-based manufacturing. Unlike the cVAE, which encodes both the design space and the design target, the UcVAE encodes only the design space. In the encoder of the UcVAE, the number of training parameters is significantly reduced compared to the cVAE, resulting in a shorter training time while maintaining comparable performance. Given desired pattern images, the trained UcVAE can generate multiple process condition solutions that produce high-fidelity hierarchical patterns.

1. Introduction

In natural systems, structural complexity imparts organisms with unique characteristics that adorn biological materials and are critical to their survival. These multiscale structural patterns originate from highly symmetrical initial states and develop during the growth and maturation of the organism [1]. Similarly, synthetic materials with hierarchical architectures that integrate the domains of hard and soft materials along strong interfaces demonstrate superior properties compared to uniform architectures [2, 3]. The bio-inspired hierarchical patterns and structures in synthetic materials are usually created through multi-step manufacturing processes such as layer-by-layer assembly [4], or additive manufacturing methods [5, 6], which require an a priori design and active intervention throughout the manufacturing process. Other manufacturing processes involving autonomous routes based on synthetic coupled reaction-mass transport processes have been explored [7–10], but these approaches are limited to solutions, gels, or thin membranes due to the prohibitively slow mass transport in solid media.

Recently, a novel manufacturing approach based on frontal polymerization (FP) was introduced, drawing parallels with morphogenic growth and development. This method enables the autonomous formation of architected pattern structures within polymeric materials [11–14]. FP is an out-of-autoclave, self-sustaining curing process that allows for rapid and energy-efficient manufacturing of thermoset polymers [15, 16]. Although stable front propagation in a homogeneous process configuration allows for the rapid production of thermoset polymeric materials [16, 17], disturbances in the system, such as variations in initial and boundary conditions, can destabilize this planar mode. This destabilization can result in front propagation instabilities, leading to the formation of complex hierarchical patterns

*Corresponding author

Email addresses: qibang@illinois.edu (Q. Liu); geubelle@illinois.edu (P. Geubelle)

within the material [18–20]. For some materials, such as cyclooctadiene (COD), FP-induced instabilities result in a spatially varying thermal history, which leads to mechanical properties that can vary by multiple orders of magnitude [11, 13].

Both stable [21–26] and unstable [11–13, 27, 28] propagation of a polymerization front in a neat resin can be described with coupled, nonlinear thermo-chemical partial differential equations (PDEs). These equations are expressed in terms of degree of cure and temperature, along with the corresponding initial and boundary conditions. Hierarchical patterns resulting from front instabilities can be obtained by solving the coupled PDEs with numerical methods, such as the finite element method (FEM), where the morphogenic pattern image is plotted based on the maximum temperature field [11–13].

Although the effect of process conditions on hierarchical patterns has been studied [13], the inverse design of process conditions to achieve a desired pattern image remains an open challenge. Designing architectural structures for specific tasks is generally a complex problem, often involving a trial-and-error approach or gradient-based optimization methods such as topology optimization [29] or genetic algorithms [30]. These methods are computationally expensive as they either use numerical methods such as FEM to solve PDEs iteratively and the performance of the search algorithms deteriorates rapidly as the design space expands. This challenge is particularly true for FP, where fine temporal and spatial discretizations are needed to capture the sharp gradients in temperature and degree of cure present near the advancing front.

Unlike traditional optimization methods, machine learning (ML)-based data-driven approaches have shown great potential in solving inverse design problems in various fields. Despite differing design targets and network architectures, a common idea is to model the relationship between design parameters and targets as a bi-directional mapping [31–34]. However, such regression problems with one-to-one mappings are inconsistent with the physical intuition that different design parameters can result in very similar design targets, which represents a one-to-many mapping. Another common approach is to use deep-learning models as surrogate models to replace computationally expensive forward simulations for search by trial-and-error or gradient-based optimizations [35–40]. Once trained, the surrogate model can predict the design target based on the design parameters in milliseconds, which is orders of magnitude faster than traditional numerical methods, thereby speeding up the inverse design trial-and-error process. Furthermore, the gradient of the design target with respect to the design parameters can be quickly and easily obtained from the surrogate model by automatic differentiation, accelerating the gradient-based optimization process. Although deep-learning surrogate models can expedite the heuristics-based design process, they still require thousands of iterations to converge to the optimal solution. More fatally, these models may have singularities in the design space, which could lead to optimization failures [41], and the gradient-based optimization process may be trapped in local minima. Therefore, forward surrogate models for iterative optimization processes are not computationally efficient or robust enough for inverse design problems.

To address these challenges, numerous probabilistic generative models have been proposed for one-to-many inverse design problems, such as conditional generative adversarial networks (cGAN) [42, 43], conditional variational autoencoders (cVAE) [44, 45], and conditional diffusion models [46–51]. These generative models can yield multiple solutions in the design space based on the design target by learning the data distribution of the typically high-dimensional design space and the usually low-dimensional design target space. However, in the hierarchical pattern design problem in FP-based morphogenic manufacturing, the design space, which describes the process conditions, is low-dimensional, whereas the design target, i.e., the pattern image, is high-dimensional.

To map one pattern image to many solutions of process conditions, we propose a novel probabilistic generative model called the univariate conditional variational autoencoder (UcVAE). Unlike the cVAE, which encodes both the design space and the design target, the UcVAE encodes only the design space. In the UcVAE encoder, the number of training parameters is significantly reduced compared to the cVAE, resulting in a shorter training time while maintaining comparable performance. Given pattern images from the test dataset generated by simulations of FEM or patterns extracted from real-world applications, trained UcVAEs for FP-based morphogenic manufacturing design can generate multiple process condition solutions that produce hierarchical patterns that closely match the target pattern images.

The paper is organized as follows: In Section 2, we describe the thermo-chemical reaction model and data generation process using FEM, the architecture of the forward model that predicts the pattern based on the process conditions, and both the cVAE and the proposed UcVAE models for inverse design. In Section 3, we present and discuss the results of the forward model and the inverse design models. Finally, we summarize the work and future directions in Section 4.

Table 1

Cure kinetics and material properties of COD [28].

$\kappa \left(\frac{\text{W}}{\text{mK}} \right)$	$\rho \left(\frac{\text{kg}}{\text{m}^3} \right)$	$C_p \left(\frac{\text{J}}{\text{kgK}} \right)$	$A \left(\frac{1}{\text{s}} \right)$
0.133	882	1838.5	2.13×10^{19}
$E \left(\frac{\text{kJ}}{\text{mol}} \right)$	n	m	$H_r \left(\frac{\text{J}}{\text{g}} \right)$
132	2.514	0.817	220.0

2. Methods

2.1. Thermo-chemical reaction model and data generation

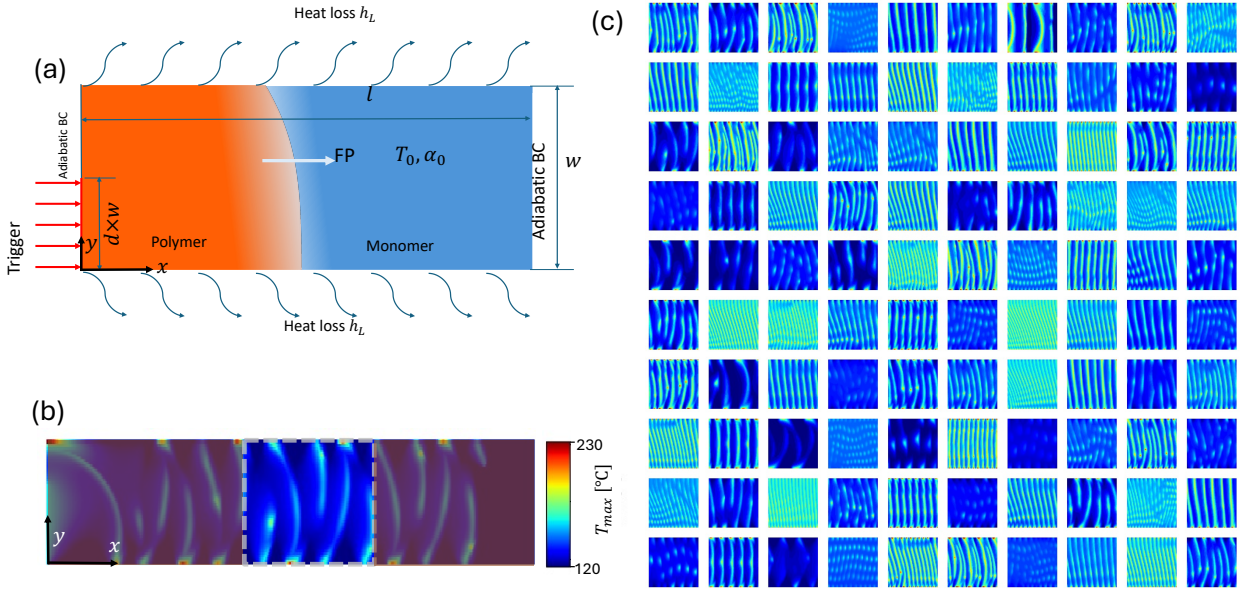


Fig. 1: FEM simulation and data generation. (a) problem setup, (b) window of interest, (c) 100 typical pattern examples out of the 4752 total samples.

The frontal polymerization of cyclooctadiene (COD) can result in hierarchical patterns [11, 13]. The initiation and propagation of the polymerization front in COD can be described by the following coupled thermo-chemical reaction-diffusion equations, expressed in terms of the degree of cure α and temperature T :

$$\begin{cases} \kappa \nabla^2 T + \rho H_r \frac{\partial \alpha}{\partial t} = \rho C_p \frac{\partial T}{\partial t}, \\ \frac{\partial \alpha}{\partial t} = A \exp\left(-\frac{E}{RT}\right) (1 - \alpha)^n \alpha^m, \end{cases} \quad (1)$$

where κ is the thermal conductivity, ρ is the density, H_r represents the total enthalpy of reaction, and C_p denotes the specific heat capacity. The second equation in Eq. (1) describes the cure kinetics of the FP reaction, with A representing the pre-exponential factor, E the activation energy, and R the universal gas constant. We use the Prout-Tompkins cure kinetics model, $(1 - \alpha)^n \alpha^m$, to describe the reaction order. The cure kinetics parameters A , E , n , and m are obtained from nonlinear fitting of heat flow measurements from differential scanning calorimetry (DSC) tests [11]. The material properties and cure kinetics parameters for COD are listed in Table 1.

The FP initiation and propagation simulations presented in this manuscript pertain to the 2D problem shown schematically in Fig. 1(a). In this setup, a polymerization front is initiated by a thermal trigger applied along the lower part of left edge with a length of $d \times w$ of a rectangular channel with dimensions $l \times w$. Once initiated, the polymerization front propagates to the right. A convective boundary condition is applied along the top and bottom of the reaction channel to capture heat loss to the surrounding. The initial and boundary conditions used to complete the

problem description are:

$$T(x, y, 0) = T_0, \quad \alpha(x, y, 0) = \alpha_0, \quad 0 \leq x \leq l, \quad 0 \leq y \leq w \quad (2a)$$

$$T(0, y, t) = T_{\text{trig}}, \quad 0 \leq y \leq d \times w, \quad t \geq 0 \quad (2b)$$

$$\frac{\partial T}{\partial x}(0, y, t) = 0, \quad d \times w < y \leq w, \quad t \geq 0 \quad (2c)$$

$$\frac{\partial T}{\partial x}(l, y, t) = 0, \quad 0 < y \leq w, \quad t \geq 0 \quad (2d)$$

$$\kappa \frac{\partial T}{\partial y}(x, y, t) = -h_L(T - T_0), \quad 0 \leq x \leq l, \quad t \geq 0, \quad y = 0 \text{ or } w. \quad (2e)$$

Here, $l = 20$ mm and $w = 5$ mm are the length and width of the channel, respectively, while $T_{\text{trig}} = 160$ °C denotes the trigger temperature. In this work, the process conditions are defined by the initial temperatures T_0 , the initial degrees of cure α_0 , the thermal trigger length fraction d , and the convective heat loss coefficient h_L .

The coupled thermal-chemical reaction-diffusion equations in Eq. (1) are solved using the finite element method (FEM) and the simulation is terminated when the front reaches 90% of the channel length. The maximum temperature $T_{\text{max}}(x, y) = \max_{t>0} \{T(x, y, t)\}$ is recorded at each point of the domain during the simulations. Once the FP is completed, the hierarchical pattern is extracted based on the T_{max} field [11, 13] and plotted using a color spectrum, as shown in Fig. 1(b). In this spectrum, dark blue represents the lower temperature bound of 120 °C and dark red represents the upper bound of 230 °C, with the number of intervals set to 30. We then extract patterns (see Fig. 1(b)) from the central part of the channel (7.5 mm $\leq x \leq 12.5$ mm) since the thermal trigger occurs at the beginning of the channel and the

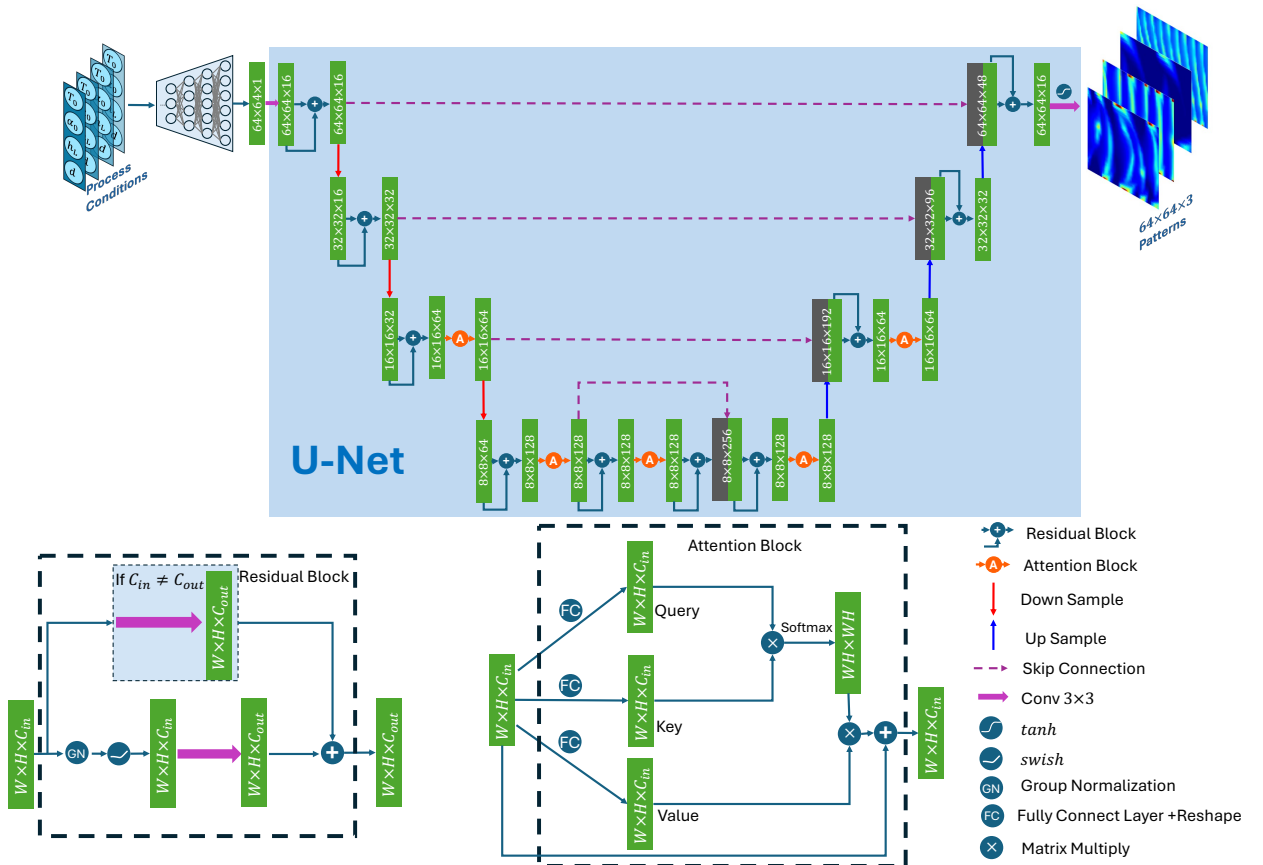


Fig. 2: Forward model linking the four process conditions to the morphogenic pattern.

last 10% of the channel is not cured. The pattern image in this region is then resized to 64×64 pixels with three RGB channels.

Varying the process conditions, such as the initial temperature T_0 , the initial degree of cure α_0 , heat loss to the surrounding h_L , and the thermal trigger length d , results in different patterns. We use the Sobol sequence with scrambling in the space of $T_0 \in [10, 40]$ °C, $\alpha_0 \in [0.01, 0.3]$, $h_L \in [0, 120]$ W/m^2K , and $d \in [0.3, 1.0]$ to sample the process conditions, thereby generating 3538 patterns by solving the PDE with FEM. However, low values of T_0 and d and high values of α_0 and h_L may lead to the quenching of front propagation, resulting in invalid patterns. We filter out 1462 valid patterns, yielding a valid percentage of 41.3%. We then estimate the mean value and the covariance matrix of the process conditions of the valid patterns to build a multivariate normal distribution. Sampling process conditions from this distribution increases the valid percentage to 89.9%. Finally, we obtain a total of 4752 samples, with Fig. 1(c) showing 100 of them. Such data generation was performed using the FEM solver FeniCS [52], on BEOCAT, a Rocky Linux-based machine at Kansas State University. Approximately 100 simulations were run simultaneously with a total of ~800 CPUs, with each simulation taking around 6.3 hours with 8 CPUs.

2.2. Forward model

We first developed a forward model to predict the pattern image based on the process conditions to validate the results from the inverse design model. To predict a high-dimensional pattern image ($64 \times 64 \times 3$) based on low-dimensional process conditions with only four input parameters, a fully connected neural network is first used to encode the process conditions. The output is reshaped into a $64 \times 64 \times 1$ image, which is then fed into a U-Net to predict the pattern image.

The U-Net [53] is a convolutional neural network (CNN) architecture commonly used for image segmentation tasks. To ensure stable training as the network depth increases, residual blocks of convolutional layers [54] were used to replace some of the U-Net architecture's building blocks [55]. These residual blocks significantly mitigate the issue of vanishing and exploding gradients commonly found in deep networks. Group normalization (GN) [56] is used to normalize the feature maps, and the swish activation function is used for nonlinearity in the residual blocks. An attention mechanism [57] is incorporated at two low levels of the U-Net to adaptively learn attention-aware features. The output of the U-Net is the pattern image with 64×64 pixels and three RGB channels.

The TensorFlow framework was used to implement the forward model, and the Adam optimizer was used to minimize the mean squared error (MSE) loss function. The schematic of the forward model, including the fully connected layers, U-Net, residual blocks, and attention blocks, is shown in Fig. 2. Further details of the implementation can be found in the Github repository.

2.3. Inverse design

The major goal of this work is to develop a model for the inverse design of morphogenic manufacturing patterns in FP due to thermo-chemical instabilities. Treating pattern design as a regression problem with a one-to-one mapping contradicts physical intuition, as different process conditions can result in very similar unstable responses and patterns, which is a one-to-many mapping.

To address this issue, we introduce latent variables as a probabilistic representation of pattern design by incorporating a conditional variational autoencoder (cVAE) architecture, first proposed by Sohn et al. [58]. As presented in Fig. 3(a), the cVAE encodes the process conditions (x) along with the corresponding patterns (y) into a latent space (z). The encoder defines a posterior distribution $q_\phi(z|x, y)$ (where ϕ denotes the parameters of the encoder), which is used to sample latent variables z from the latent space. By imposing a specific prior distribution $p_\theta(z)$ on the latent space, multiple designed process conditions can be reconstructed from the latent variables sampled within the latent space, enabling these varied designs to produce similar target patterns.

The generative model, also named the decoder, defines the generative distribution of the process conditions (x) given the target patterns (y) and latent variables (z), $p_\theta(x|y, z)$ (where θ denotes the parameters of the decoder), which is used for the inverse design in this work. Within the inverse design process, a set of latent variables z are sampled from the prior distribution $p_\theta(z)$, and a set of process conditions are then generated by the decoder given the target pattern y and the latent variables z . These generated process conditions are fed into the forward model or FEM simulation to obtain the designed pattern images, which should be similar to the given target pattern image.

The training objective of the cVAE model is to maximize the likelihood of the conditional probability $p_\theta(x|y)$, given the training dataset, as described in [58]:

$$\max\{\log p_\theta(x|y)\} = \max\{L_{vbl}(x, y; \theta, \phi)\}, \quad (3)$$

where $L_{vbl}(x, y; \theta, \phi)$ is the variational lower bound (VLB) and is defined as

$$L_{vbl}(x, y; \theta, \phi) = \mathbb{E}_{q_{\phi}(z|x)} [\log p_{\theta}(x|y, z)] - \text{KL} [q_{\phi}(z|x, y) || p_{\theta}(z)]. \quad (4)$$

In this relation, KL denotes the Kullback-Leibler divergence, which describes the discrepancy between the two distributions. Training the cVAE and maximizing the VLB is equivalent to minimizing the negative VLB, which leads to the loss function of the cVAE model

$$(\theta, \phi) = \arg \min_{\theta, \phi} \{-L_{vbl}(x, y; \theta, \phi)\} = \arg \min_{\theta, \phi} L_{loss}, \quad (5)$$

where the loss function L_{loss} is defined as

$$L_{loss} = ||x - \hat{x}|| + \text{KL} [q_{\phi}(z|x, y) || p_{\theta}(z)]. \quad (6)$$

The term $||x - \hat{x}||$ denotes the reconstruction loss, which measures the difference between the input process condition and the generated process condition.

In this cVAE-based inverse design neural network architecture shown in Fig. 3(a), we need to encode and decode the pattern images, whose dimension is as high as $64 \times 64 \times 3$. U-Net architectures are a prevalent choice, and we use the same U-Net architecture as in the forward model. The process condition is low-dimensional, with only four parameters, so a simple fully connected neural network is used to encode the process conditions. The output is concatenated with the output of the U-Net and then fed into another fully connected neural network, whose outputs are the mean and standard deviation of the latent space distribution with a dimension of two. In the decoder, the latent variables are

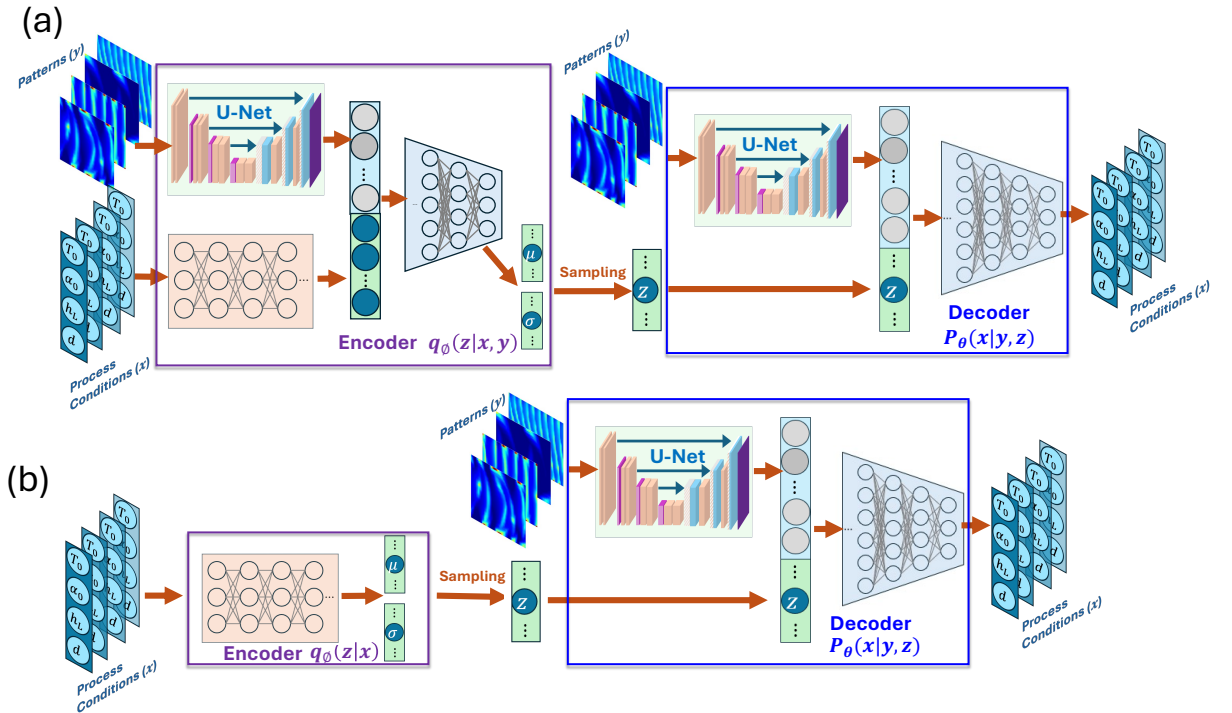


Fig. 3: Neural network architecture for inverse design, where the U-Net architecture is the same as the one in the forward model. (a) Conditional variational autoencoder (cVAE) for inverse design, encoding both the design targets (patterns y) and the design parameters (process conditions x), originally proposed by Sohn et al. [58]. The encoder and decoder have 2,158,711 and 2,166,256 training parameters, respectively. (b) Univariate conditional variational autoencoder (UCVAE) proposed in this work for the inverse pattern design, encoding only the design parameters. The encoder and decoder have 644 and 2,166,256 training parameters, respectively.

sampled from the latent space distribution, concatenated with the output of the U-Net, and fed into a fully connected neural network to output the predicted process conditions.

In this cVAE model, the encoder and decoder have 2,158,711 and 2,166,256 training parameters, respectively, whereas the U-Net has 2.06 million training parameters and constitutes the major part of both the encoder and decoder. We use a large U-Net because a large model is needed to extract the features of the high-dimensional pattern image, while the process conditions include only four parameters, so a small model is sufficient to encode the process conditions. Thus, we propose a novel cVAE for inverse design, which only encodes the generative variables (i.e., process conditions x), but not the conditions (i.e., pattern images y). We refer to this cVAE as univariate cVAE (UcVAE) because only the generative variables are encoded, as shown in Fig. 3(b).

Since we do not encode the pattern images using the U-Net, the encoder is a simple fully connected neural network with only 644 training parameters. The encoder defines a proposed posterior distribution $q_\phi(z|x)$. The decoder of the UcVAE is the same as the cVAE, which defines a generative distribution $p_\theta(x|y, z)$, and the true posterior is $p_\theta(z|x, y)$. The KL divergence describes the discrepancy between the proposed and true posterior distributions as

$$\text{KL} [q_\phi(z|x)||p_\theta(z|x, y)] = \mathbb{E}_{q_\phi(z|x)} [\log q_\phi(z|x) - \log p_\theta(z|x, y)]. \quad (7)$$

The optimization objective of the UcVAE model is also to maximize the likelihood of the conditional probability $p_\theta(x|y)$, which is equivalent to minimizing the negative VLB. The VLB for the UcVAE is derived as follows:

$$\begin{aligned} \log p_\theta(x|y) &> \log p_\theta(x|y) - \text{KL} [q_\phi(z|x)||p_\theta(z|x, y)] \\ &= \mathbb{E}_{q_\phi(z|x)} [\log p_\theta(x|y)] - \mathbb{E}_{q_\phi(z|x)} \left[\log \frac{q_\phi(z|x)}{p_\theta(z|x, y)} \right] \\ &= \mathbb{E}_{q_\phi(z|x)} \left[-\log \frac{q_\phi(z|x)}{p_\theta(x|y)p_\theta(z|x, y)} \right] \\ &= \mathbb{E}_{q_\phi(z|x)} \left[-\log \frac{q_\phi(z|x) p_\theta(x, y)}{p_\theta(x|y) p_\theta(zxy)} \right] \\ &= \mathbb{E}_{q_\phi(z|x)} \left[-\log \frac{q_\phi(z|x) p_\theta(y, z) p_\theta(y) p_\theta(x, y)}{p_\theta(x|y) p_\theta(zxy) p_\theta(y, z) p_\theta(y)} \right] \\ &= \mathbb{E}_{q_\phi(z|x)} \left[-\log \frac{q_\phi(z|x)}{p_\theta(x|y)} \frac{1}{p_\theta(x|y, z)} \frac{1}{p_\theta(z|y)} p_\theta(x|y) \right] \\ &= \mathbb{E}_{q_\phi(z|x)} \left[-\log \frac{q_\phi(z|x)}{p_\theta(z|y)} + \log p_\theta(x|y, z) \right] \\ &= \mathbb{E}_{q_\phi(z|x)} [\log p_\theta(x|y, z)] - \text{KL} [q_\phi(z|x)||p_\theta(z)] \\ &= L_{vbl}(x, y; \theta, \phi). \end{aligned} \quad (8)$$

The negative VLB leads to the loss function of the UcVAE model as

$$L_{loss} = ||x - \hat{x}|| + \text{KL} [q_\phi(z|x)||p_\theta(z)]. \quad (9)$$

Once the model is trained, the encoder is no longer needed. The decoder can be transferred to a machine as a standalone model to infer multiple solutions (x) almost instantly based on one target (y) but various latent variables (z), for specific generative tasks such as practical quick design optimization in industrial workflows. In this work, we developed the UcVAE for FP-based morphogenic manufacturing design, but it can also be used for many other generative tasks. For further details on the implementation of the cVAE and UcVAE in this work, please refer to our Github repository.

3. Results and discussion

In this section, we present the results of the forward model and the inverse design models. The total dataset generated using FEM simulation was shuffled and divided into 80% training data and 20% test data to train the forward and inverse models. Neural network training was performed on a single Nvidia A100 GPU on DELTA, a Red Hat

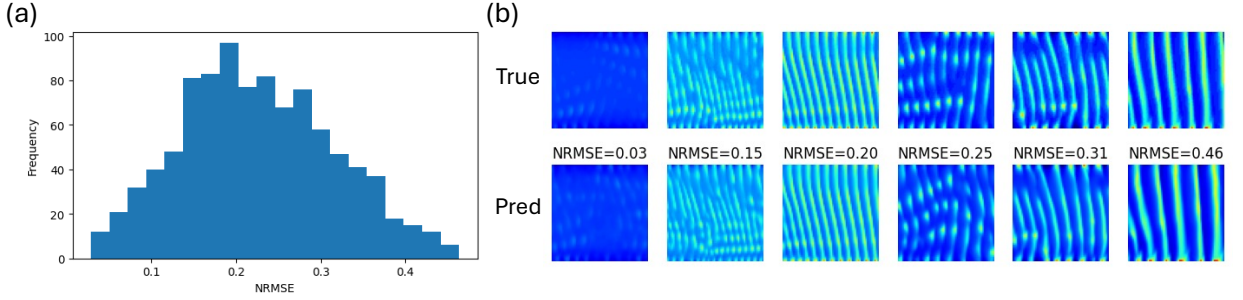


Fig. 4: Forward model performance. (a) Normalized root mean squared error (NRMSE) of the test dataset. (b) Comparison between predicted and true patterns of the test dataset, arranged from best (left) to worst (right).

Enterprise Linux-based machine at the National Center for Supercomputing Applications at the University of Illinois Urbana-Champaign. For model performance evaluation, the normalized root mean squared error (NRMSE) from the `skimage` package is used:

$$\text{NRMSE} = \frac{\|y^{\text{true}} - y^{\text{pred}}\|_2}{y_{\text{max}}^{\text{true}} - y_{\text{min}}^{\text{true}}}. \quad (10)$$

3.1. Forward model performance

The forward model is trained with 1600 epochs using the Adam optimizer with a learning rate of 5.0×10^{-4} and a batch size of 128. Each epoch takes 2.2 seconds for training. After training, it takes only 270 ms to predict the 951 test pattern images. The distribution of NRMSE over all test samples is presented in Fig. 4(a), showing a maximum NRMSE of 0.46. The average value and standard deviation of the NRMSE distribution for the test samples are 0.23 and 0.09, respectively. Fig. 4(b) displays a comparison between the true patterns and their corresponding predictions. The patterns are evenly arranged from best (left image) to worst (right image). As shown in that figure, even in the worst prediction with an NRMSE of 0.46, the forward model predicts the pattern image quite accurately. This well-trained forward model is then used to evaluate the performance of the generative inverse model.

3.2. Inverse design performance

Two neural network architectures are developed for the inverse design of FP-based morphogenic manufacturing patterns. One is based on the original cVAE architecture, which encodes both the process conditions and the pattern images, with an encoder having 2,158,711 training parameters. The other is the proposed UcVAE architecture, which only encodes the process conditions with an encoder having only 644 training parameters. Both the cVAE and UcVAE are trained for 900 epochs using the Adam optimizer with a learning rate of 5.0×10^{-4} and a batch size of 128.

Fig. 5(a) and (c) show the MSE loss values during the training process for cVAE and UcVAE, respectively. As apparent in these figures, the reconstruction losses of both the UcVAE and cVAE are comparable, but the KL divergence of the UcVAE is an order of magnitude lower than that of the cVAE.

Once the neural networks are trained, the designed process conditions are generated by sampling one latent variable from the prior standard normal distribution for each design target pattern sample in the test dataset. The designed process conditions are then fed into the forward model to obtain the designed pattern images, which are compared with the corresponding design target pattern images. The NRMSE distribution over the test targets is shown in Fig. 5(b) and (d) for cVAE and UcVAE, respectively. As apparent in Fig. 5, the NRMSE distributions of cVAE and UcVAE are similar. The average NRMSE value for cVAE is 0.1858, which is slightly larger than that for UcVAE, 0.1849. The standard deviations for cVAE and UcVAE are also similar: 0.0995 and 0.1014, respectively.

We randomly selected 40 design targets from the test dataset and show in Fig. 6 the design results obtained with cVAE and UcVAE. As apparent there, the two approaches yield predictions with patterns similar to the targets. Both Fig. 5 and Fig. 6 show that UcVAE and cVAE achieve similar design performance. However, because UcVAE only encodes the process conditions into the latent space and has far fewer training parameters than cVAE, training UcVAE takes only 1.8 seconds per epoch, which is 50% less than the 3.6 seconds per epoch required for cVAE.

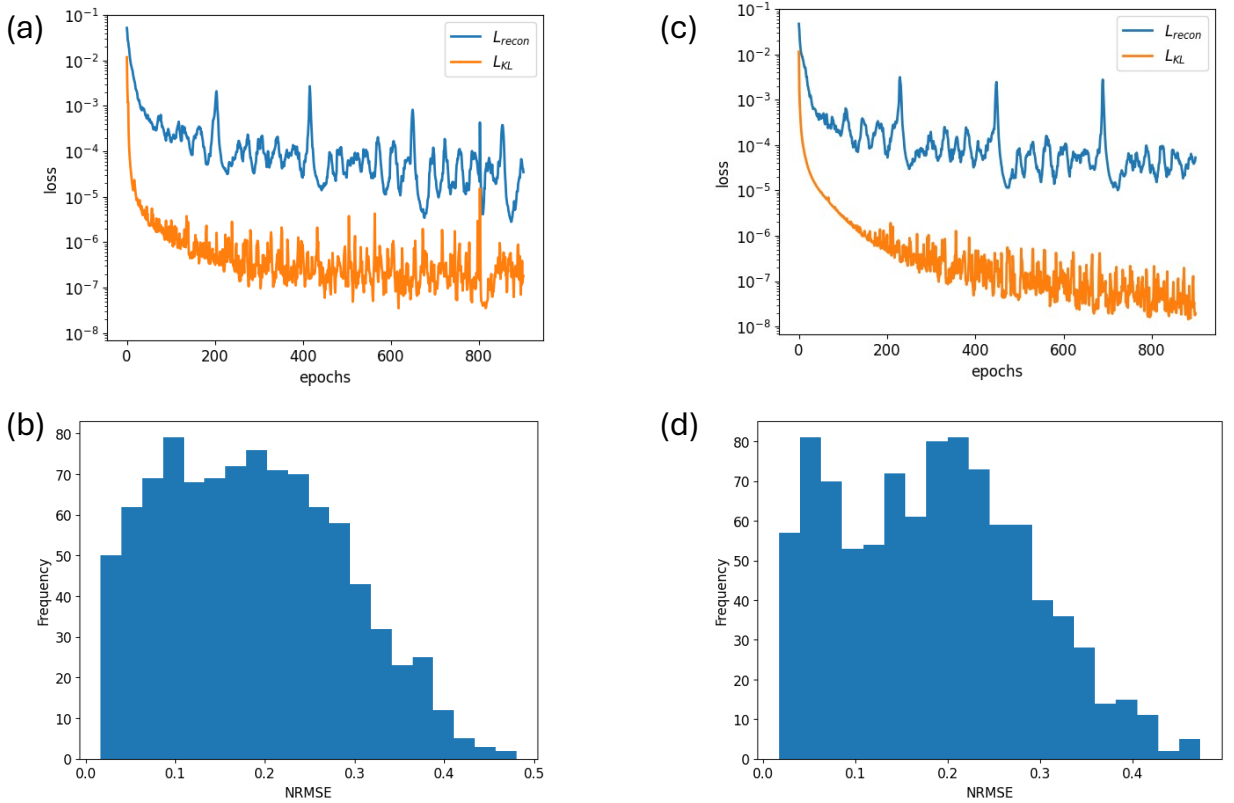


Fig. 5: Model performance of inverse design. Loss values during the training process for cVAE (a) and UcVAE (c). NRMSE between target pattern image from the test dataset and corresponding designed pattern image obtained with cVAE (b) and UcVAE (d). In these figures, one random latent vector z following a standard normal distribution is used to generate one process condition for each sample, and the process conditions are fed into the forward model to obtain the design images.

3.3. One-to-many inverse design

The generative neural networks can be used for one-to-many solutions, allowing multiple solutions to be generated for a given target. In this section, we demonstrate the one-to-many inverse design of FP-based morphogenic manufacturing patterns using the UcVAE. For a well-trained UcVAE, the encoder is no longer needed and only the decoder is used for inverse design. For a given design target, changing the latent variables z will result in different process conditions that can produce designed images very close to the target image. In the following inverse design tasks, the latent variables z are not sampled from a standard normal distribution but from a Sobol sequence with scrambling in the space of $[-64, 64]$ to achieve more diverse design solutions.

We randomly selected from the test dataset the 3 design targets shown in Fig. 7(a1), (b1), and (c1). For each design target, we sampled 1024 latent variables z from the Sobol space. By feeding the design target and the 1024 latent variables into the decoder of the UcVAE, we obtained 1024 designed process conditions for each design target, as shown in Fig. 7(a2), (b2), and (c2). The designed process conditions were then fed into the forward model to obtain the designed pattern images. The NRMSE computed through comparison to the target is shown as a color map in Fig. 7(a2), (b2), and (c2), with the blue triangle representing the best design process conditions. Fig. 7(a3), (b3), and (c3) show the designed pattern images predicted by the forward model with the designed process conditions, arranged from best (left) to worst (right) in terms of NRMSE. As indicated in these figures, the designed pattern images associated with the three design targets and obtained from various designed process conditions are very close to the target images. Fig. 7(a4), (b4), and (c4) show the designed pattern images obtained from FEM simulation with the best design process conditions, which are also very close to the target images. These one-to-many inverse design results demonstrate that the UcVAE can generate multiple solutions for a given target.

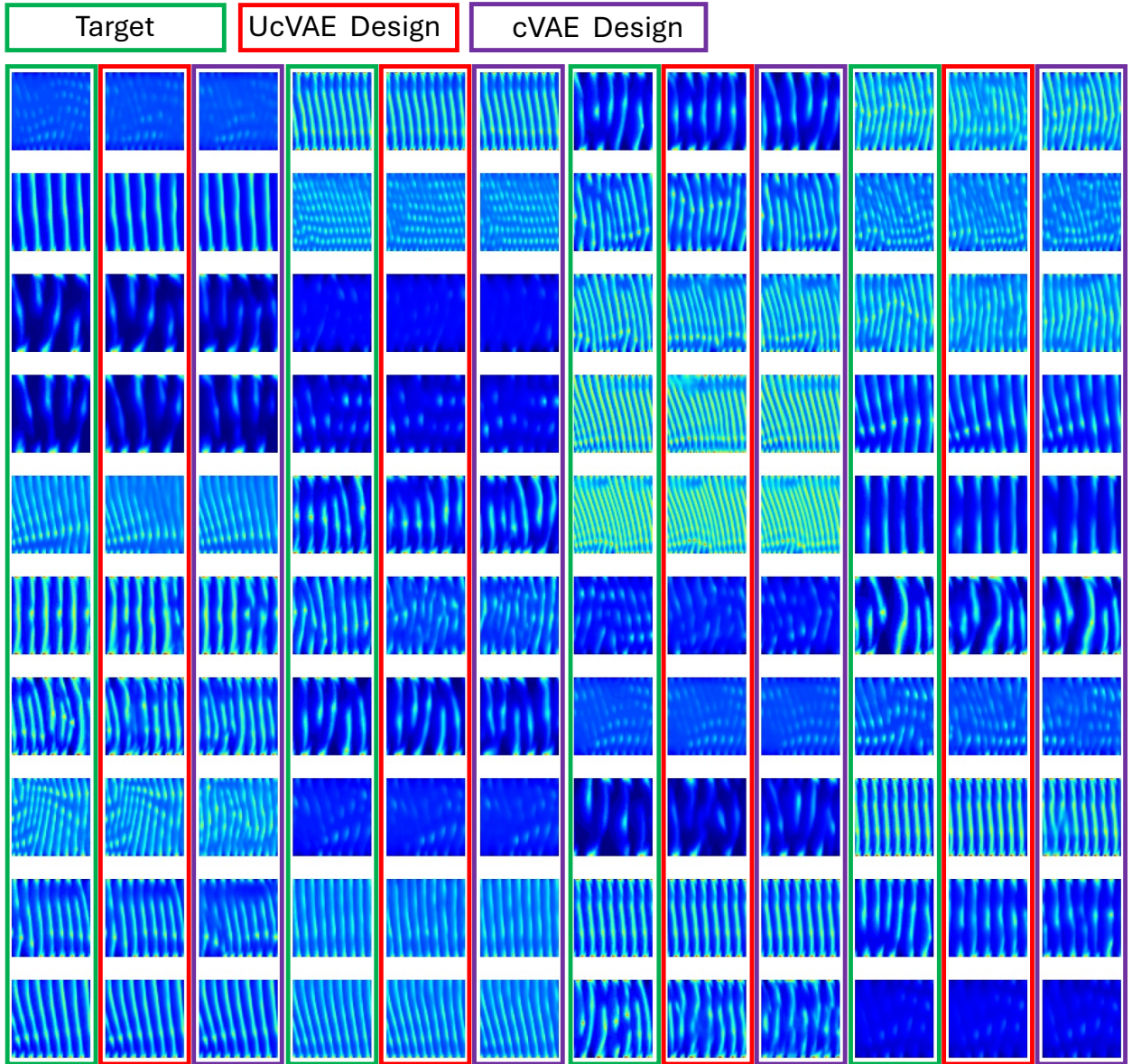


Fig. 6: Forty random design examples obtained by UcVAE (red frames) and cVAE (purple frames). The targets (green frames) are random samples from the test dataset. One random latent vector z following a standard normal distribution is used to generate one process condition for each sample, and the process conditions are fed into the forward model to obtain the design images.

While our developed UcVAE performs well on the test dataset for inverse retrieval, real-world applications often demand on-the-fly inverse design of custom-defined patterns with high fidelity. Therefore, instead of strictly achievable patterns such as those shown in Fig. 7, a robust inverse design model should be able to generate possible designs from a rough sketch of predefined patterns. Thus, instead of FEM simulation-generated patterns, we now use real-world patterns as design targets for on-demand inverse design. We adopt the patterns shown in Fig. 8. Fig. 8(a1), (b1), and (c1). Fig. 8(a1) shows an experimentally observed FP-induced pattern described in [13], Fig. 8(b1) is a SEM image of a cross-section through a typical spicule in a laminated architecture taken from [59], and Fig. 8(c1) shows ripples of sand taken from nature.

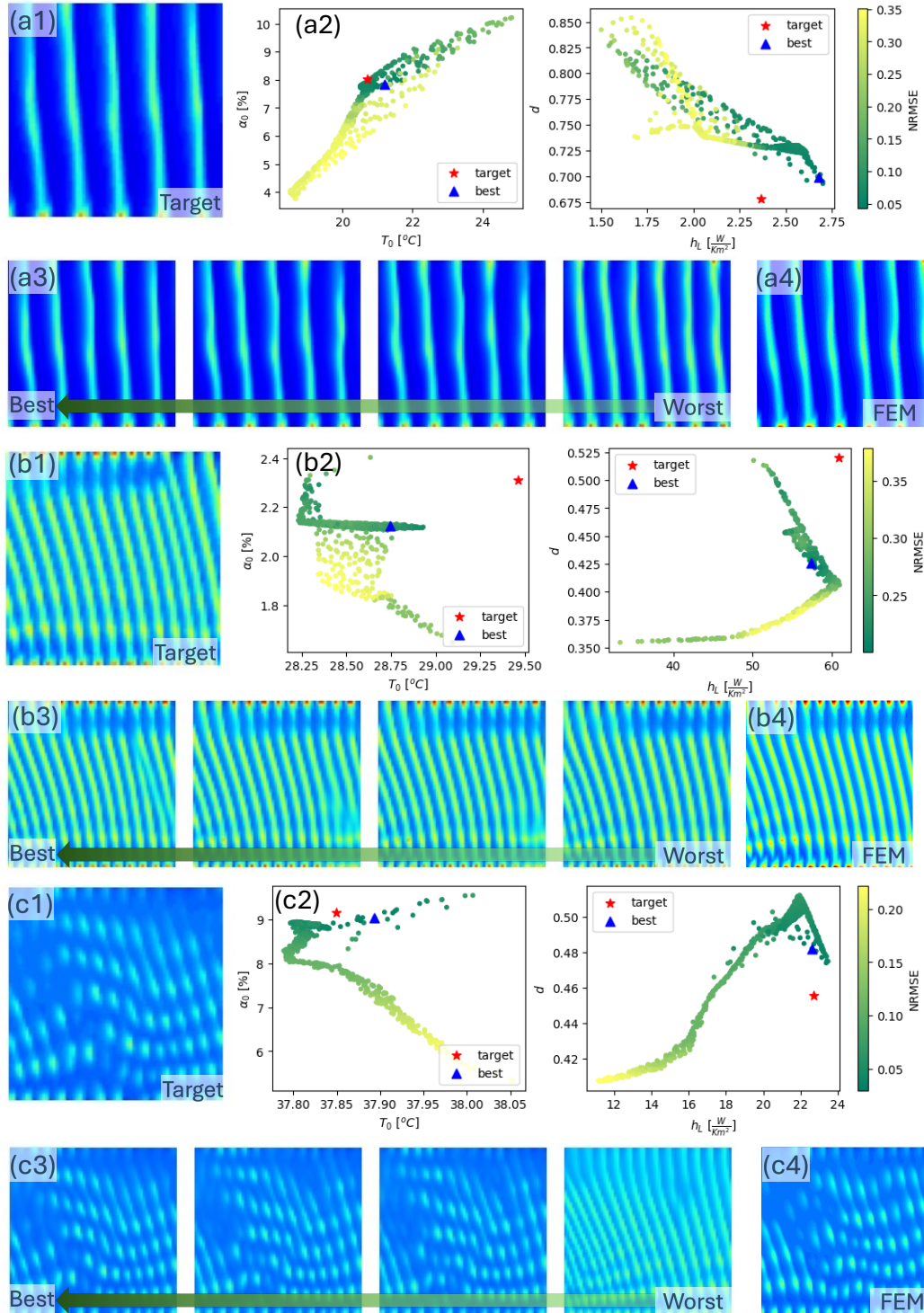


Fig. 7: One-to-many inverse design of patterns using UcVAE. (a1), (b1), (c1) show random design targets from the test dataset. (a2), (b2), (c2) display 1024 designed process conditions generated by UcVAE with 1024 random latent vectors z in Sobol space. (a3), (b3), (c3) present the designed pattern images predicted by the forward model with the designed process conditions, arranged from best (left) to worst (right) in terms of NRMSE, where the best design process conditions are indicated by the blue triangle in (a2), (b2), (c2). (a4), (b4), (c4) show the designed pattern images obtained from FEM simulation with the best design process conditions.

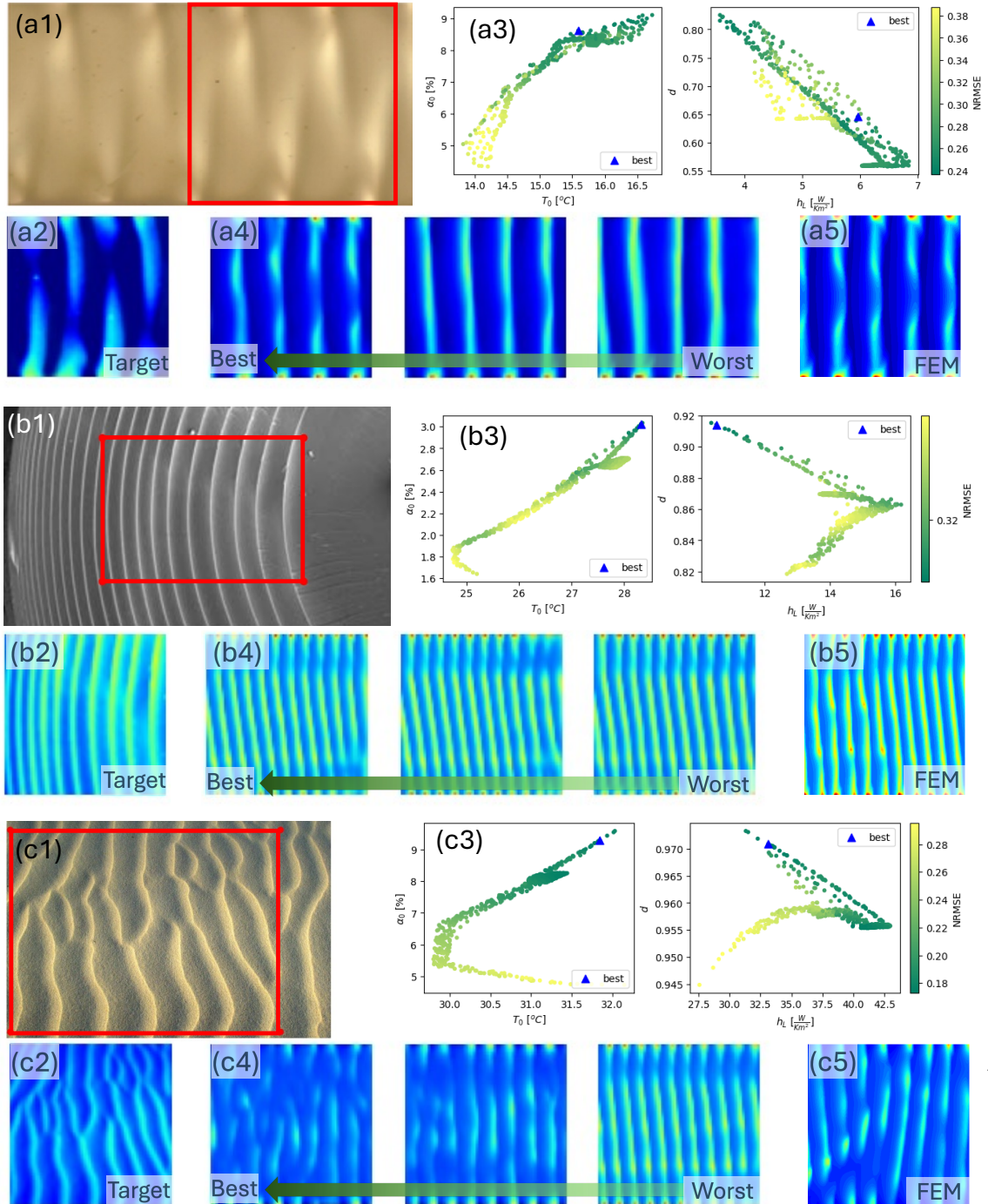


Fig. 8: On-demand one-to-many inverse design of patterns using UcVAE. (a1), (b1), (c1) show real-world patterns from an experiment, an SEM image of a typical spicule, and an image of ripples of sand from nature, respectively. (a2), (b2), (c2) are the RGB design target patterns extracted from (a1), (b1), (c1), respectively. (a3), (b3), (c3) display 1024 designed process conditions generated by UcVAE with 1024 random latent vectors z in Sobol space. (a4), (b4), (c4) present the designed pattern images predicted by the forward model with the designed process conditions, arranged from best (left) to worst (right) in terms of NRMSE, where the best design process conditions are indicated by the blue triangle in (a3), (b3), (c3). (a5), (b5), (c5) show the designed pattern images obtained from FEM simulation with the best design process conditions.

These real-world pattern images are cropped along the red window shown in Fig. 8(a1), (b1), and (c1), then converted to RGB images with color spectrum and resized to 64×64 pixels, as shown in Fig. 8(a2), (b2), and (c2). Similar to the inverse design of the samples from the test dataset shown in Fig. 7, we sample 1024 latent variables z from Sobol space for the design target from the real-world patterns, and then feed the design target and the 1024 latent variables into the decoder of the UcVAE. The designed process conditions are shown in Fig. 8(a3), (b3), and (c3), where the blue triangle represents the best design process conditions.

Predicted design pattern images by the forward model with the designed process conditions are shown in Fig. 8(a4), (b4), and (c4), arranged from best (left) to worst (right) in terms of NRMSE. Fig. 8(a5), (b5), and (c5) show the designed pattern images obtained from FEM simulation with the best design process conditions. As apparent from Fig. 8, the designed pattern images from the real-world patterns are roughly close to the target images. The difference in patterns is mainly due to the model being trained with FEM simulation-generated data, whose distribution is quite different from the real-world patterns.

The three on-demand inverse design examples in Fig. 8 demonstrate the ability of the developed UcVAE to generate multiple solutions for a given custom-defined target pattern, with the designed pattern images exhibiting rough fidelity to the target images.

4. Conclusions and future work

In this work, we have proposed a novel probabilistic generative model named univariate conditional variational autoencoder (UcVAE) to conditionally generate multiple solutions. Unlike the more classical conditional variational autoencoder (cVAE), which encodes both the solution space and the specific target, the UcVAE encodes only the solution space. This significantly reduces the number of training parameters in the encoder, resulting in a shorter training time while maintaining comparable performance.

We developed and trained a UcVAE-based neural network architecture incorporating U-Net, ResNet, and attention mechanisms for the inverse design of hierarchical patterns in FP-based manufacturing. The encoder of the UcVAE has only 644 training parameters, compared to the cVAE's 2,158,711 parameters. Training the UcVAE takes only 1.8 seconds per epoch, which is 50% less than the cVAE's 3.6 seconds per epoch, while achieving similar design performance. For a given design target from the test dataset generated by FEM simulation, the UcVAE can generate multiple solutions that produce hierarchical patterns very close to the target images. Beyond strictly feasible patterns generated by FEM simulation, three real-world patterns have also been used as the design target for on-demand inverse design. In that more challenging case, the UcVAE also generated multiple solutions that produce hierarchical patterns with acceptable fidelity.

Beyond the inverse design of morphogenic manufacturing patterns in FP, the proposed UcVAE can be applied to many other generative tasks. Future work include broadening the morphogenic manufacturing design space by incorporating more complex chemical compositions and extending pattern designs from numerical simulations to other manufacturing processes.

Code availability

The codes and data that support the findings of this study are available from the GitHub repository at <https://github.com/QibangLiu/UcVAE>.

CRedit authorship contribution statement

Qibang Liu: Writing – review & editing, Writing – original draft, Software, Methodology, Formal analysis, Conceptualization, Resources. **Pengfei Cai:** Writing – review & editing, Investigation, Conceptualization. **Diab Abueidda:** Writing – review & editing, Investigation, Resources. **Sagar Vyas:** Writing – review & editing, Investigation, Conceptualization. **Seid Koric:** Writing – review & editing, Investigation, Resources. **Rafael Gomez-Bombarelli:** Writing – review & editing, Supervision, Funding acquisition. **Philippe Geubelle:** Writing – review & editing, Supervision, Methodology, Funding acquisition, Conceptualization.

Conflict of interest

The authors declare that they have no conflict of interest.

Acknowledgments

This work was supported as part of the Regenerative Energy-Efficient Manufacturing of Thermoset Polymeric Materials (REMAT), an Energy Frontier Research Center funded by the U.S. Department of Energy, Office of Science, Basic Energy Sciences under award DE-SC0023457.

The authors would like to thank the National Center for Supercomputing Applications (NCSA) at the University of Illinois, and particularly its Research Computing Directorate, Industry Program, and Center for Artificial Intelligence Innovation (CAII) for support and hardware resources. This research is a part of the Delta research computing project, which is supported by the National Science Foundation (award OCI 2005572) and the State of Illinois, as well as the Illinois Computes program supported by the University of Illinois Urbana-Champaign and the University of Illinois System.

The data generation by FEM simulation for this project was performed on the Beocat Research Cluster at Kansas State University.

References

- [1] D. Melton, Pattern formation during animal development, *Science* 252 (1991) 234–241. doi:10.1126/science.1672778.
- [2] W. Huang, D. Restrepo, J.-Y. Jung, F. Y. Su, Z. Liu, R. O. Ritchie, J. McKittrick, P. Zavattieri, D. Kisailus, Multiscale toughening mechanisms in biological materials and bioinspired designs, *Advanced Materials* 31 (2019) 1901561. doi:10.1002/adma.201901561.
- [3] A. K. Rylski, H. L. Cater, K. S. Mason, M. J. Allen, A. J. Arrowood, B. D. Freeman, G. E. Sanoja, Z. A. Page, Polymeric multimaterials by photochemical patterning of crystallinity, *Science* 378 (2022) 211–215. doi:10.1126/science.add6975.
- [4] J. J. Richardson, J. Cui, M. Bjornmalm, J. A. Braunger, H. Ejima, F. Caruso, Innovation in layer-by-layer assembly, *Chemical reviews* 116 (2016) 14828–14867. doi:10.1021/acs.chemrev.6b00277.
- [5] R. L. Truby, J. A. Lewis, Printing soft matter in three dimensions, *Nature* 540 (2016) 371–378. doi:10.1038/nature21003.
- [6] M. Saadi, A. Maguire, N. T. Pottackal, M. S. H. Thakur, M. M. Ikram, A. J. Hart, P. M. Ajayan, M. M. Rahman, Direct ink writing: a 3d printing technology for diverse materials, *Advanced Materials* 34 (2022) 2108855. doi:10.1002/adma.202108855.
- [7] C. J. Campbell, M. Fialkowski, R. Klajn, I. T. Bensemann, B. A. Grzybowski, Color micro-and nanopatterning with counter-propagating reaction–diffusion fronts, *Advanced Materials* 16 (2004) 1912–1917. doi:10.1002/adma.200400383.
- [8] C. J. Campbell, R. Klajn, M. Fialkowski, B. A. Grzybowski, One-step multilevel microfabrication by reaction–diffusion, *Langmuir* 21 (2005) 418–423. doi:10.1021/la0487747.
- [9] D. Karig, K. M. Martini, T. Lu, N. A. DeLateur, N. Goldenfeld, R. Weiss, Stochastic turing patterns in a synthetic bacterial population, *Proceedings of the National Academy of Sciences* 115 (2018) 6572–6577. doi:10.1073/pnas.1720770115.
- [10] Z. Tan, S. Chen, X. Peng, L. Zhang, C. Gao, Polyamide membranes with nanoscale turing structures for water purification, *Science* 360 (2018) 518–521. doi:10.1126/science.aar6308.
- [11] E. M. Lloyd, E. C. Feinberg, Y. Gao, S. R. Peterson, B. Soman, J. Hemmer, L. M. Dean, Q. Wu, P. H. Geubelle, N. R. Sottos, et al., Spontaneous patterning during frontal polymerization, *ACS central science* 7 (2021) 603–612. doi:10.1021/acscentsci.1c00110.
- [12] Y. Gao, M. A. Dearborn, J. Hemmer, Z. Wang, A. P. Esser-Kahn, P. H. Geubelle, Controllable frontal polymerization and spontaneous patterning enabled by phase-changing particles, *Small* 17 (2021) 2102217. doi:10.1002/smll.202102217.
- [13] J. E. Paul, Y. Gao, Y. K. Go, L. E. Rodriguez Koett, A. Sharma, M. Chen, J. J. Lessard, T. Topkaya, C. Leal, J. S. Moore, P. H. Geubelle, N. R. Sottos, Controlled patterning of crystalline domains by frontal polymerization, *Nature* (2024). doi:10.1038/s41586-024-07951-7.
- [14] J. S. Moore, P. H. Geubelle, N. R. Sottos, E. C. Firestone, E. M. Lloyd, Method of spontaneously patterning a polymer during frontal polymerization, 2024. US Patent App. 18/265,141.
- [15] J. A. Pojman, V. M. Ilyashenko, A. M. Khan, Free-radical frontal polymerization: Self-propagating thermal reaction waves, *Journal of the Chemical Society, Faraday Transactions* 92 (1996) 2825–2837. doi:10.1039/ft9969202825.
- [16] I. D. Robertson, M. Yourdkhani, P. J. Centellas, J. E. Aw, D. G. Ivanoff, E. Goli, E. M. Lloyd, L. M. Dean, N. R. Sottos, P. H. Geubelle, et al., Rapid energy-efficient manufacturing of polymers and composites via frontal polymerization, *Nature* 557 (2018) 223–227. doi:10.1038/s41586-018-0054-x.
- [17] A. Mariani, S. Fiori, Y. Chekanov, J. A. Pojman, Frontal ring-opening metathesis polymerization of dicyclopentadiene, *Macromolecules* 34 (2001) 6539–6541. doi:10.1021/ma0106999.
- [18] J. A. Pojman, V. M. Ilyashenko, A. M. Khan, Spin mode instabilities in propagating fronts of polymerization, *Physica D: Nonlinear Phenomena* 84 (1995) 260–268. doi:10.1016/0167-2789(95)00022-V.
- [19] J. Masere, F. Stewart, T. Meehan, J. A. Pojman, Period-doubling behavior in frontal polymerization of multifunctional acrylates, *Chaos: An Interdisciplinary Journal of Nonlinear Science* 9 (1999) 315–322. doi:10.1063/1.166408.
- [20] V. M. Ilyashenko, J. A. Pojman, Single-head spin modes in frontal polymerization, *Chaos: An Interdisciplinary Journal of Nonlinear Science* 8 (1998) 285–289. doi:10.1063/1.166311.
- [21] E. Goli, I. D. Robertson, P. H. Geubelle, J. S. Moore, Frontal polymerization of dicyclopentadiene: a numerical study, *The Journal of Physical Chemistry B* 122 (2018) 4583–4591. doi:10.1021/acs.jpcc.7b12316.
- [22] E. Goli, N. Parikh, M. Yourdkhani, N. Hibbard, J. Moore, N. Sottos, P. Geubelle, Frontal polymerization of unidirectional carbon-fiber-reinforced composites, *Composites Part A: Applied Science and Manufacturing* 130 (2020) 105689. URL: <https://linkinghub.elsevier.com/retrieve/pii/S1359835X19304385>. doi:10.1016/j.compositesa.2019.105689.

- [23] S. Vyas, X. Zhang, E. Goli, P. Geubelle, Frontal vs. bulk polymerization of fiber-reinforced polymer-matrix composites, *Composites Science and Technology* 198 (2020) 108303. URL: <https://linkinghub.elsevier.com/retrieve/pii/S026635382030498X>. doi:10.1016/j.compscitech.2020.108303.
- [24] M. Garg, J. E. Aw, X. Zhang, P. J. Centellas, L. M. Dean, E. M. Lloyd, I. D. Robertson, Y. Liu, M. Yourdkhani, J. S. Moore, et al., Rapid synchronized fabrication of vascularized thermosets and composites, *Nature communications* 12 (2021) 2836. doi:10.1038/s41467-021-23054-7.
- [25] Y. Gao, L. E. Rodriguez Koett, J. Hemmer, T. Gai, N. A. Parikh, N. R. Sottos, P. H. Geubelle, Frontal polymerization of thin layers on a thermally insulating substrate, *ACS Applied Polymer Materials* 4 (2022) 4919–4927. URL: <https://pubs.acs.org/doi/10.1021/acscapm.2c00497>.
- [26] Q. Liu, D. Abueidda, S. Vyas, Y. Gao, S. Koric, P. H. Geubelle, Adaptive data-driven deep-learning surrogate model for frontal polymerization in dicyclopentadiene, *The Journal of Physical Chemistry B* 128 (2024) 1220–1230. doi:10.1021/acs.jpcc.3c07714.
- [27] E. Goli, S. Peterson, P. Geubelle, Instabilities driven by frontal polymerization in thermosetting polymers and composites, *Composites Part B: Engineering* 199 (2020) 108306. URL: <https://linkinghub.elsevier.com/retrieve/pii/S1359836820333539>. doi:10.1016/j.compositesb.2020.108306.
- [28] Y. Gao, M. A. Dearborn, S. Vyas, A. Kumar, J. Hemmer, Z. Wang, Q. Wu, O. Alshangiti, J. S. Moore, A. P. Esser-Kahn, et al., Manipulating frontal polymerization and instabilities with phase-changing microparticles, *The Journal of Physical Chemistry B* 125 (2021) 7537–7545. doi:10.1021/acs.jpcc.1c03899.
- [29] J. Andkjær, S. Nishiwaki, T. Nomura, O. Sigmund, Topology optimization of grating couplers for the efficient excitation of surface plasmons, *JOSA B* 27 (2010) 1828–1832. doi:10.1364/JOSAB.27.001828.
- [30] M. D. Huntington, L. J. Lauhon, T. W. Odom, Subwavelength lattice optics by evolutionary design, *Nano letters* 14 (2014) 7195–7200. doi:10.1021/nl5040573.
- [31] D. Liu, Y. Tan, E. Khoram, Z. Yu, Training deep neural networks for the inverse design of nanophotonic structures, *Acs Photonics* 5 (2018) 1365–1369. doi:10.1021/acsp Photonics.7b01377.
- [32] W. Ma, F. Cheng, Y. Liu, Deep-learning-enabled on-demand design of chiral metamaterials, *ACS nano* 12 (2018) 6326–6334. doi:10.1021/acsnano.8b03569.
- [33] L. Gao, X. Li, D. Liu, L. Wang, Z. Yu, A bidirectional deep neural network for accurate silicon color design, *Advanced Materials* 31 (2019) 1905467. doi:10.1002/adma.201905467.
- [34] E. Goli, S. Vyas, S. Koric, N. Sobh, P. H. Geubelle, Chemnet: A deep neural network for advanced composites manufacturing, *The Journal of Physical Chemistry B* 124 (2020) 9428–9437. doi:10.1021/acs.jpcc.0c03328.
- [35] T. Chugh, C. Sun, H. Wang, Y. Jin, Surrogate-assisted evolutionary optimization of large problems, *High-Performance Simulation-Based Optimization* (2020) 165–187. doi:10.1007/978-3-030-18764-4_8.
- [36] S. D. Campbell, D. Z. Zhu, E. B. Whiting, J. Nagar, D. H. Werner, P. L. Werner, Advanced multi-objective and surrogate-assisted optimization of topologically diverse metasurface architectures, in: *Metamaterials, Metadevices, and Metasystems 2018*, volume 10719, SPIE, 2018, pp. 43–48. doi:10.1117/12.2321159.
- [37] R. S. Hegde, Photonics inverse design: pairing deep neural networks with evolutionary algorithms, *IEEE Journal of Selected Topics in Quantum Electronics* 26 (2019) 1–8. doi:10.1109/JSTQE.2019.2933796.
- [38] Z. A. Kudyshev, A. V. Kildishev, V. M. Shalaev, A. Boltasseva, Machine learning-assisted global optimization of photonic devices, *Nanophotonics* 10 (2020) 371–383. doi:10.1515/nanoph-2020-0376.
- [39] H. T. Kollmann, D. W. Abueidda, S. Koric, E. Guleryuz, N. A. Sobh, Deep learning for topology optimization of 2d metamaterials, *Materials & Design* 196 (2020) 109098. doi:10.1016/j.matdes.2020.109098.
- [40] D. W. Abueidda, S. Koric, N. A. Sobh, Topology optimization of 2d structures with nonlinearities using deep learning, *Computers & Structures* 237 (2020) 106283. doi:10.1016/j.compstruc.2020.106283.
- [41] P. R. Wiecha, A. Arbouet, C. Girard, O. L. Muskens, Deep learning in nano-photonics: inverse design and beyond, *Photonics Research* 9 (2021) B182–B200. doi:10.1364/PRJ.415960.
- [42] Z. Liu, D. Zhu, S. P. Rodrigues, K.-T. Lee, W. Cai, Generative model for the inverse design of metasurfaces, *Nano letters* 18 (2018) 6570–6576. doi:10.1021/acs.nanolett.8b03171.
- [43] S. So, J. Rho, Designing nanophotonic structures using conditional deep convolutional generative adversarial networks, *Nanophotonics* 8 (2019) 1255–1261. doi:10.1515/nanoph-2019-0117.
- [44] W. Ma, F. Cheng, Y. Xu, Q. Wen, Y. Liu, Probabilistic representation and inverse design of metamaterials based on a deep generative model with semi-supervised learning strategy, *Advanced Materials* 31 (2019) 1901111. doi:10.1002/adma.201901111.
- [45] K. Yonekura, K. Suzuki, Data-driven design exploration method using conditional variational autoencoder for airfoil design, *Structural and Multidisciplinary Optimization* 64 (2021) 613–624. doi:10.1007/s00158-021-02851-0.
- [46] J.-H. Bastek, D. M. Kochmann, Inverse design of nonlinear mechanical metamaterials via video denoising diffusion models, *Nature Machine Intelligence* 5 (2023) 1466–1475. doi:10.1038/s42256-023-00762-x.
- [47] T. Weiss, E. Mayo Yanes, S. Chakraborty, L. Cosmo, A. M. Bronstein, R. Gershoni-Poranne, Guided diffusion for inverse molecular design, *Nature Computational Science* 3 (2023) 873–882. doi:10.1038/s43588-023-00532-0.
- [48] N. N. Vlassis, W. Sun, Denoising diffusion algorithm for inverse design of microstructures with fine-tuned nonlinear material properties, *Computer Methods in Applied Mechanics and Engineering* 413 (2023) 116126. doi:10.1016/j.cma.2023.116126.
- [49] I. Igashov, H. Stärk, C. Vignac, A. Schneuing, V. G. Satorras, P. Frossard, M. Welling, M. Bronstein, B. Correia, Equivariant 3d-conditional diffusion model for molecular linker design, *Nature Machine Intelligence* (2024) 1–11. doi:10.1038/s42256-024-00815-9.
- [50] J. Park, A. P. S. Gill, S. M. Moosavi, J. Kim, Inverse design of porous materials: a diffusion model approach, *Journal of Materials Chemistry A* 12 (2024) 6507–6514. doi:10.1039/d3ta06274k.

- [51] J. Park, S. Kushwaha, J. He, S. Koric, Q. Liu, I. Jasiuk, D. Abueidda, Nonlinear inverse design of mechanical multi-material metamaterials enabled by video denoising diffusion and structure identifier, arXiv preprint arXiv:2409.13908 (2024). doi:/10.48550/arXiv.2409.13908.
- [52] M. Alnæs, J. Blechta, J. Hake, A. Johansson, B. Kehlet, A. Logg, C. Richardson, J. Ring, M. E. Rognes, G. N. Wells, The fenics project version 1.5, *Archive of Numerical Software* 3 (2015). doi:10.11588/ans.2015.100.20553.
- [53] O. Ronneberger, P. Fischer, T. Brox, U-net: Convolutional networks for biomedical image segmentation, in: *Medical image computing and computer-assisted intervention—MICCAI 2015: 18th international conference, Munich, Germany, October 5-9, 2015, proceedings, part III 18*, Springer, 2015, pp. 234–241. doi:10.1007/978-3-319-24574-4_28.
- [54] K. He, X. Zhang, S. Ren, J. Sun, Identity mappings in deep residual networks, in: *Computer Vision—ECCV 2016: 14th European Conference, Amsterdam, The Netherlands, October 11–14, 2016, Proceedings, Part IV 14*, Springer, 2016, pp. 630–645. doi:10.1007/978-3-319-46493-0_38.
- [55] F. I. Diakogiannis, F. Waldner, P. Caccetta, C. Wu, Resunet-a: A deep learning framework for semantic segmentation of remotely sensed data, *ISPRS Journal of Photogrammetry and Remote Sensing* 162 (2020) 94–114. doi:10.1016/j.isprsjprs.2020.02.013.
- [56] Y. Wu, K. He, Group normalization, in: *Proceedings of the European conference on computer vision (ECCV)*, 2018, pp. 3–19. doi:10.1007/978-3-030-01234-2_1.
- [57] A. Vaswani, Attention is all you need, *Advances in Neural Information Processing Systems* (2017). doi:10.5555/3295222.3295349.
- [58] K. Sohn, H. Lee, X. Yan, Learning structured output representation using deep conditional generative models, *Advances in neural information processing systems* 28 (2015).
- [59] J. Aizenberg, J. C. Weaver, M. S. Thanawala, V. C. Sundar, D. E. Morse, P. Fratzl, Skeleton of euplectella sp.: structural hierarchy from the nanoscale to the macroscale, *Science* 309 (2005) 275–278. doi:10.1126/science.1112255.